256 GBd Barium-Titanate-on-SiN Mach-Zehnder Modulator

Manuel Kohli[1], Daniel Chelladurai[1], Laurenz Kulmer[1], Killian Keller[1], Yannik Horst[1], Tobias Blatter[1], Joel Winiger[1], David Moor[1], Tatiana Buriakova[2], Michael Zervas[2], Clarissa Convertino[3], Felix Eltes[3], Yuriy Fedoryshyn[1], Ueli Koch[1], and Juerg Leuthold[1]

[1]ETH Zurich, Institute of Electromagnetic Fields (IEF), Gloriastrasse 35, 8092 Zurich, Switzerland

[2]Ligentec SA, 1024 Ecublens, Switzerland

[3]Lumiphase AG, Laubisrütistrasse 44, 8712 Stäfa, Switzerland

Author e-mail address: manuel.kohli@ief.ee.ethz.ch, juerg.leuthold@ief.ee.ethz.ch

Abstract: We demonstrate a 110-GHz BTO Mach-Zehnder modulator integrated on foundry-produced silicon nitride for 340 Gbit/s data links. This approach, featuring nano-scale plasmonics and highly nonlinear BTO, proves to be a viable platform for next-generation Tbit/s links.

1. Introduction

High-speed modulators with symbol rates beyond 100 GBd are essential to build next-generation Tbit/s links [1, 2]. Ideally, a modulator not only reaches high speeds, but also has a small footprint, low energy consumption [3], and is compatible with versatile and low-loss photonic platform such as silicon nitride (SiN) [4].

Photonic modulators based on thin-film lithium niobate (TFLN) show great performance, reaching a symbol rate of 260 GBd in an IQ modulator [5] and 510 Gbit/s net bitrate for baseband modulation [6]. To decrease the typically large footprint of photonic modulators, there exist two main possibilities: increase the electro-optic interaction or utilize materials with higher nonlinearity. The first can be achieved with plasmonic modulators. Plasmonic-organic-hybrid (POH) modulators with a bandwidth of up to 500 GHz have been demonstrated [7], while achieving 256 GBd and 774 Gbit/s in an IQ modulator [8]. The second route to miniaturization can for example be accomplished by the ferroelectric material barium titanate (BTO), which offers up to 30 times larger Pockels effect than TFLN [9–11]. To date, photonic BTO Mach-Zehnder modulators have reached 112 GBd in 4PAM with a voltage-length product ($V_{\pi}L$) of 5.76 Vmm [12]. First plasmonic BTO modulators have achieved 72 GBd with 10 µm long devices [13]. While these demonstrations are impressive, the integration of modulators with high-performance photonic platforms, that offer advanced applications, is increasingly required [14]. As such, the SiN platform is gaining in popularity. It offers negligible two-photon absorption, lower loss, larger thermal stability, and a larger transparency window in comparison to silicon [14–17]. Yet, active components are still rare on this emerging platform. Examples include TFLN/SiN modulators reaching 80 GBd in 2PAM [18] and 64 GBd in 4PAM [19]. Benefiting from a shorter wavelength ($\lambda =$ 784 nm), a 110-GHz TFLN modulator has been shown [20]. Recently, a first BTO on SiN modulator has demonstrated operation up to 216 GBd [4]. Nevertheless, demonstrations with data links beyond 300 Gbit/s are missing to date.

In this work, we demonstrate a 110-GHz plasmonic BTO modulator on SiN that features a length of 15 µm, a low $V_{\pi,\mathrm{DC}}L$ of 0.027 Vmm and $V_{\pi,40\mathrm{GHz}}L = 0.096$ Vmm in push-pull configuration. It offers bitrates exceeding 300 Gbit/s and a record symbol rate with BTO of 256 GBd 2PAM in intensity-modulation with direct-detection (IM/DD). Furthermore, we demonstrate data experiments reaching 256 GBd over a 400 m fiber link.

2. Design and Fabrication

The plasmonic BTO modulator on SiN, see Fig. 1, consists of two phase shifters in a balanced configuration. We utilize amorphous silicon gratings to couple into the SiN [21]. The light is split into the two arms of the MZM with a multi-mode interferometer. The operating point of the MZM is set by applying a current through a platinum heater

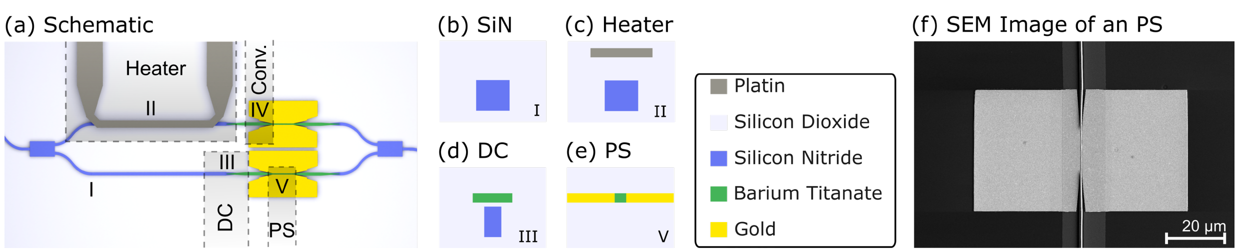

Fig. 1. (a) Schematic of the MZM. (b)-(e) Different cross-sections in the modulator. Position I in (a) corresponds to (b), II to (c), III to (d), and V to (e), respectively. (f) SEM image of a BTO plasmonic phase shifter (PS).

located above the 800×800 nm SiN waveguide, see Fig. 1(c). The light is then guided in both arms to an 800×220 nm fully etched BTO waveguide by tapering both the SiN and the BTO, see Fig. 1(d). Finally, the light is guided into a 150 nm wide plasmonic slot in a 14 µm long converter similarly to [4], see Fig. 1(e).

The photonic SiN waveguides were defined, etched, and planarized prior to a wafer-scaled integration of BTO. The modulator itself was fabricated by etching the BTO after being patterned with electron-beam lithography (EBL) to form the waveguides and the plasmonic slot. Amorphous silicon was deposited and etched using plasma-enhanced chemical vapor deposition, EBL, and reactive-ion etching for the grating couplers. In the next step, gold was deposited and afterwards SiO_2 was used as a cladding. The heaters were fabricated by depositing platinum. Fig. 1(f) shows an SEM image of a fabricated BTO plasmonic phase shifter.

3. Modulator Performance

In this section, we describe the performance of the modulator. First, the modulator was characterized optically and electro-optically. Then, we show the results of the data transmission experiments with 2PAM, 4PAM, and 8PAM, in addition to a 400 m fiber transmission using 2PAM and 4PAM.

The DC $V_{\pi,\mathrm{DC}}$ of the MZM in push-pull configuration is 1.8 V. This was determined by applying a voltage to the phaseshifters of the MZM and monitoring the optical output. The optical extinction ratio is measured by applying a current to the heater and is found to be 13.3 dB. Fig. 2(c) shows the measured frequency response of the modulator as normalized modulation efficiency from the peak-to-sideband ratio. The drop from 10 MHz to roughly 15 GHz corresponds to a lowering of the electro-optical coefficient in BTO seen in plasmonic devices, leading to a $V_{\pi,\mathrm{RF}} =$ 6.4 V [11]. We measure the frequency characteristics of the modulator in three steps using an RF generator between 10 MHz to 67 GHz and an RF mixer between 70 GHz and 110 GHz. The continuity between the two measurements is verified with a wideband signal generated with an arbitrary waveform generator (AWG). The modulation efficiency was captured with an optical spectrum analyzer.

Simulations predict fiber-to-fiber insertion losses (IL) below 10 dB for this plasmonic modulator. This includes 1.25 dB for the grating couplers, <0.1 dB for the interlayer transition, <1 dB for the photonic-to-plasmonic convertor, and finally 0.3 dB/µm propagation losses in the 15 µm long plasmonic slot. In experiment, we measure a total IL of 20.3 dB. Through cutback measurements, a propagation loss of 4.5 dB/cm is calculated in BTO waveguides. The interlayer transition loss from SiN to the BTO waveguide is 0.14 dB per transition. The grating couplers are measured to be 2.8 dB per coupler. Furthermore, cutback measurements show 0.5 dB/µm propagation losses for the plasmonic section. This leaves roughly 3.5 dB per photonic-to-plasmonic converter. Fabrication improvements in the metallization step and to the grating couplers promise about 10 dB loss reduction for future implementations.

The setup of the data transmission experiment is shown in Fig. 2. A tunable laser source (TLS) coupled with an erbium-doped fiber amplifier (EDFA) generated the optical carrier (20.5 dBm) at $\lambda = 1550$ nm. A periodically repeated square root raised cosine bit sequence was generated for up to 256 GBd signal rate by an AWG. To align the domains of the BTO, 3 V_{DC} was applied to the modulator. The heater was utilized to set the MZM operating point. The receiver, see Fig. 2(b), consists of an EDFA, a filter, and a photodetector. The signal is then captured with a real-time digital sampling oscilloscope (DSO) for a direct detection scheme. A 400 m long fiber was included after the SiN chip for the fiber transmission experiment. The offline digital signal processing (DSP) consists of a timing recovery, a T/2-spaced linear equalization (LMS) with 151 taps, a nonlinear equalization based on a 7-symbol pattern mapping (MAP), and finally a second T-spaced LMS with 251 taps. For the 8PAM, the MAP was reduced to 5-symbols and the second T-spaced LMS was increased to 1001 taps. For the 4PAM format, a third order Volterra was added prior to the 7-symbol pattern mapping, while the second LMS was kept constant at 251 taps. For the measurements with the simplified DSP, only a timing recovery and a T/2-spaced LMS with 151 taps was applied.

The results from the data transmission experiment can be seen in Fig. 3. In (a), the eye diagram of the 256 GBd 2PAM data signal is shown with a bit-error ratio (BER) of $2.67 \cdot 10^{-2}$ and an SNR of 7.58 dB. (b) shows 340 Gbit/s line

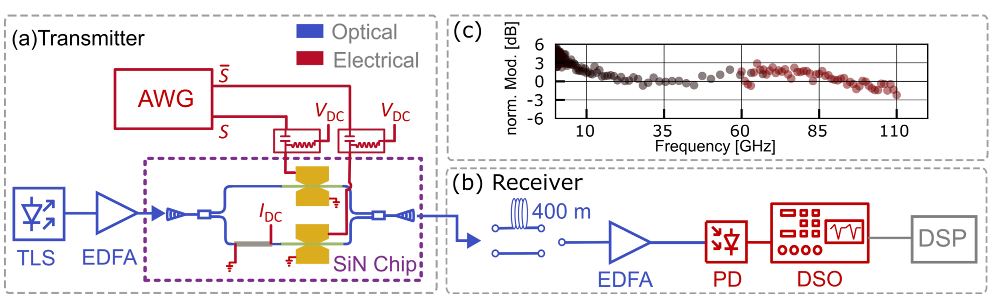

Fig. 2. (a) Measurement setup for the transmitter. (b) Measurement setup of the receiver for the data experiment. (c) Frequency response of the modulator. It shows the expected drop between 10 MHz and 20 GHz. The modulator response flattens to reach 110 GHz.

rate of the 4PAM signal with BER of $3.75 \cdot 10^{-2}$ and SNR of 12.18 dB, (c) of the 96 GBd 8PAM signal with a BER of $3.98 \cdot 10^{-2}$ and an SNR of 15.3 dB, and (c) of the 160 GBd 4PAM with simplified DSP and a BER of $3.24 \cdot 10^{-2}$ and SNR of 11.72 dB. The eye diagram of the 400 m fiber transmission experiment is shown in (e) for the 2PAM (BER of $3.1 \cdot 10^{-2}$, SNR of 7.29 dB) and (f) for 4PAM (BER of $4.00 \cdot 10^{-2}$, SNR of 12 dB). In (e), the BER is shown as a function of the transmitted symbol rate. The color of the lines represents the modulation format, where the circles show the simplified DSP (timing recovery and a 151 LMS only). The full DSP is represented with the crosses. For the 2PAM signal, simple DSP can be utilized below 160 GBd for quasi-error-free (BER < $1 \cdot 10^{-5}$) communication and up to 196 GBd below the SD-FEC limit with 20 % overhead of $4 \cdot 10^{-2}$ [22]. Furthermore, for the 4PAM transmission, the simple DSP suffices for signal rates up to 96 GBd to stay below the HD-FEC limit and up to 160 GBd for the SD-FEC limit.

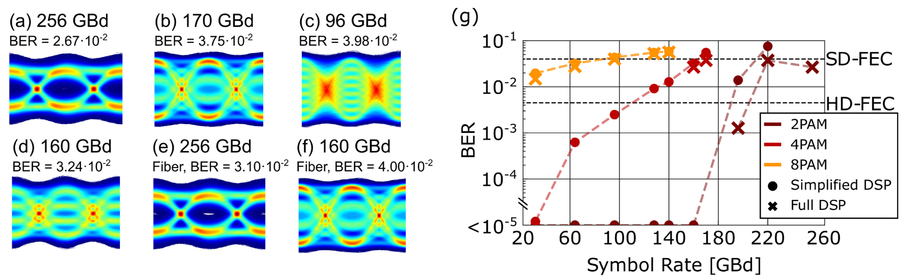

Fig. 3. (a) Eye diagram of the 2PAM 256 Gbit/s, (b) 4PAM 340 Gbit/s, (c) 8PAM 288 Gbit/s, and (d) 4PAM 320 Gbit/s line rates with simplified DSP. The eye diagram of the 400 m fiber transmission experiment is seen in (e) for the 2PAM 256 GBd and (f) for 4PAM 160 GBd. (g) Dependence of the BER on the transmitted symbol rates. The colors indicate the modulation format. Circled show simple DSP and crosses full DSP.

4. Conclusion

A high-speed BTO modulator on foundry-produced SiN is demonstrated. This integration combines the advantages of the powerful and low-loss SiN platform with the highly nonlinear BTO and nano-scale plasmonics for a 110-GHz modulator reaching 256 GBd. We demonstrate a low DC voltage-length product of 0.027 Vmm in push-pull configuration. This modulator is capable of data links beyond 300 Gbit/s, reaching 256 GBd in 2PAM, 170 GBd in 4PAM, and 96 GBd in 8PAM below the SD-FEC limit. Simplified DSP consisting of timing recovery and a 151 taps LMS only can be employed up to 196 GBd 2PAM and 160 GBd 4PAM. We further demonstrate the functionality with a fiber-transmission experiment over 400 m for 256 GBd 2PAM and 160 GBd 4PAM. This shows that our approach of a BTO-on-SiN platform is suitable for next-generation energy-efficient data links.

Acknowledgements

This work was funded by the EC H2020 projects NEBULA (871658) and PlasmoniAC (871391), and the Horizon Europe project ALLEGRO (101092766). We thank the cleanroom operations team of the Binnig and Rohrer Nanotechnology Center (BRNC) for their help and support.

5. References

[1] P. J. Winzer and D. T. Neilson, ‘From scaling disparities to integrated parallelism: A decathlon for a decade’, *JLT*, vol. 35, no. 5, pp. 1099–1115, 2017.

[2] Q. Cheng, *et al.*, ‘Recent advances in optical technologies for data centers: a review’, *Optica*, vol. 5, no. 11, pp. 1354–1370, Nov. 2018, doi: 10.1364/OPTICA.5.001354.

[3] D. A. Miller, ‘Attojoule optoelectronics for low-energy information processing and communications’, *JLT*, vol. 35, no. 3, pp. 346–396, 2017.

[4] M. Kohli *et al.*, ‘Plasmonic Ferroelectric Modulator Monolithically Integrated on SiN for 216 GBd Data Transmission’, *JLT*, pp. 1–7, 2023, doi: 10.1109/JLT.2023.3260064.

[5] H. Mardoyan *et al.*, ‘First 260-GBd single-carrier coherent transmission over 100 km distance based on novel arbitrary waveform generator and thin-film lithium niobate I/Q modulator’, in *ECOC 2022*, Optica Publishing Group, 2022, p. Th3C.2.

[6] Q. Hu and R. Borkowski, ‘510 Gbit/s Net Bitrate IM/DD Link Enabled by 200 GBd Precoded Duooctonary (1+D)-PAM-8 Modulation with Memoryless Decoding’, in *ECOC 2023*, Glasgow, Oct. 2023, p. Th1C.7.

[7] M. Burla *et al.*, ‘500 GHz plasmonic Mach-Zehnder modulator enabling sub-THz microwave photonics’, *Apl Photonics*, vol. 4, no. 5, 2019.

[8] L. Kulmer, Y. Horst, Destraz, Marcel, Blatter, Tobias, Koepfli, M. Stefan, and Leuthold, Juerg, ‘256 GBd Single-Carrier Transmission over 100km SSMF by a Plasmonic IQ Modulator’, in *ECOC 2023*, Glasgow, Oct. 2023, p. We5D.5.

[9] M. Zgonik *et al.*, ‘Dielectric, elastic, piezoelectric, electro-optic, and elasto-optic tensors of $BaTiO_3$ crystals’, *Phys. Rev. B*, vol. 50, no. 9, pp. 5941–5949, Sep. 1994, doi: 10.1103/PhysRevB.50.5941.

[10] S. Abel *et al.*, ‘Large Pockels effect in micro- and nanostructured barium titanate integrated on silicon’, *Nature Mater*, vol. 18, no. 1, Art. no. 1, Jan. 2019, doi: 10.1038/s41563-018-0208-0.

[11] J. Winiger *et al.*, ‘PLD Epitaxial Thin-Film BaTiO3 on MgO − Dielectric and Electro-Optic Properties’, *Advanced Materials Interfaces*, vol. n/a, no. n/a, p. 2300665, doi: 10.1002/admi.202300665.

[12] F. Eltes *et al.*, ‘Thin-film BTO-based modulators enabling 200 Gb/s data rates with sub 1 Vpp drive signal’, in *OFC 2023, paper Th4A.2*, Optica Publishing Group, Mar. 2023, p. Th4A.2. doi: 10.1364/OFC.2023.Th4A.2.

[13] A. Messner *et al.*, ‘Plasmonic Ferroelectric Modulators’, *JLT.*, vol. 37, no. 2, pp. 281–290, Jan. 2019, doi: 10.1109/JLT.2018.2881332.

[14] Q. Wilmart *et al.*, ‘A Versatile Silicon-Silicon Nitride Photonics Platform for Enhanced Functionalities and Applications’, *Applied Sciences*, vol. 9, no. 2, Art. no. 2, Jan. 2019, doi: 10.3390/app9020255.

[15] C. H. Henry, R. F. Kazarinov, H. J. Lee, K. J. Orlowsky, and L. E. Katz, ‘Low loss Si3N4–SiO2 optical waveguides on si’, *Appl. Opt.*, vol. 26, no. 13, pp. 2621–2624, Jul. 1987, doi: 10.1364/AO.26.002621.

[16] R. Heideman *et al.*, ‘Large-scale integrated optics using TriPleX waveguide technology: from UV to IR’, in *Photonics Packaging, Integration, and Interconnects IX*, SPIE, Feb. 2009, pp. 203–217. doi: 10.1117/12.808409.

[17] M. H. P. Pfeiffer *et al.*, ‘Photonic Damascene Process for Low-Loss, High-Confinement Silicon Nitride Waveguides’, *IEEE Journal of Selected Topics in Quantum Electronics*, vol. 24, no. 4, pp. 1–11, Jul. 2018, doi: 10.1109/JSTQE.2018.2808258.

[18] P. Zhang *et al.*, ‘High-speed electro-optic modulator based on silicon nitride loaded lithium niobate on an insulator platform’, *Opt. Lett.*, vol. 46, no. 23, pp. 5986–5989, Dec. 2021, doi: 10.1364/OL.446222.

[19] Z. Ruan *et al.*, ‘High-Performance Electro-Optic Modulator on Silicon Nitride Platform with Heterogeneous Integration of Lithium Niobate’, *Laser & Photonics Reviews*, vol. 17, no. 4, p. 2200327, 2023, doi: 10.1002/lpor.202200327.

[20] F. Valdez, V. Mere, and S. Mookherjea, ‘100 GHz bandwidth, 1 volt integrated electro-optic Mach-Zehnder modulator at near-IR wavelengths’, *Optica, OPTICA*, vol. 10, no. 5, pp. 578–584, May 2023, doi: 10.1364/OPTICA.484549.

[21] M. Kohli *et al.*, ‘C- and O-Band Dual-Polarization Fiber-to-Chip Grating Couplers for Silicon Nitride Photonics’, *ACS Photonics*, vol. 10, no. 9, pp. 3366–3373, Sep. 2023, doi: 10.1021/acsphotonics.3c00834.

[22] K. Schuh *et al.*, ‘Single Carrier 1.2 Tbit/s Transmission over 300 km with PM-64 QAM at 100 GBaud’, in *OFC 2017*, Mar. 2017, p. Th5B.5. doi: 10.1364/OFC.2017.Th5B.5.